Accepted Manuscript

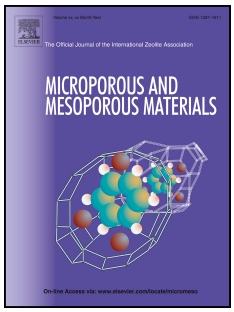

Refractive index and scattering of porous TiO_2 films

S. Abdellatif, P. Sharifi, K. Kirah, R. Ghannam, A.S.G. Khalil, D. Erni, F. Marlow

PII: S1387-1811(18)30018-0

DOI: 10.1016/j.micromeso.2018.01.011

Reference: MICMAT 8736

To appear in: *Microporous and Mesoporous Materials*

Received Date: 12 May 2017

Revised Date: 30 November 2017

Accepted Date: 10 January 2018

Please cite this article as: S. Abdellatif, P. Sharifi, K. Kirah, R. Ghannam, A.S.G. Khalil, D. Erni, F. Marlow, Refractive index and scattering of porous TiO_2 films, *Microporous and Mesoporous Materials* (2018), doi: 10.1016/j.micromeso.2018.01.011.

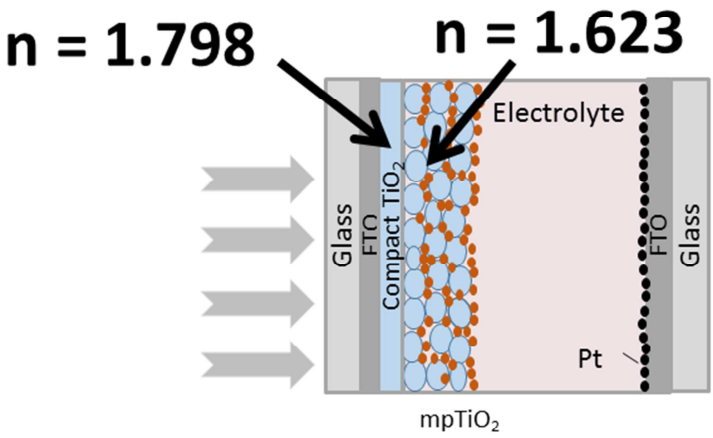

Refractive Index and Scattering of Porous TiO_2 Films

S. Abdellatif,[1,2] P. Sharifi,[3] K. Kirah,[4] R. Ghannam,[2] A. S. G. Khalil,[5,6]
D. Erni[7] and F. Marlow,[3,*]
[1]The British University in Egypt (BUE), Cairo, Egypt
[2]Egypt Nanotechnology Center, Cairo University, Giza, Egypt
[3]Max-Planck-Institut für Kohlenforschung, Mülheim, Germany
[4]Faculty of Engineering, Ain Shams University, Cairo, Egypt
[5]Arab Academy for Science, Technology and Maritime Transport, Giza, Egypt
[6]Physics Department, Faculty of Science, Fayoum University, Fayoum, Egypt
[7]General and Theoretical Electrical Engineering (ATE), Faculty of Engineering, University of Duisburg-Essen, and CENIDE - Center for Nanointegration Duisburg-Essen, Duisburg, Germany.
*Corresponding author: e-mail: marlow@mpi-muelheim.mpg.de
Mailing address: Max-Planck-Institut für Kohlenforschung, 45470 Mülheim, Germany

Abstract
Porous titanium dioxide (TiO_2) films are essential components of dye sensitized solar cells (DSSCs) as well as perovskite solar cells (PSCs). Unfortunately, porosity, refractive index, and scattering properties of these films are only roughly known. This induces uncertainties in modelling and understanding of these solar cells. Since the literature provides only descriptions of the optical properties of the porous TiO_2 layers with unclear relevance to these solar cells, we investigate porous TiO_2 films really used in DSSCs and potentially usable in PSCs. The effective refractive index and the film porosity for different nanostructures that were fabricated from solution-based techniques were determined. The found values are 1.7982 ± 0.005 for the effective refractive index of one kind of TiO_2 films and 1.62 ± 0.002 for another one. These values lead to porosities of 53.5% and 65%, respectively. The scattering of the films can be described by a wavelength-independent effective scattering parameter for one film type and by effective scattering particles with a diameter of 46.5 nm for the other film type. The determined porosities are also of relevance for the ionic transport which is functionally crucial in DSSCs and a disturbance in PSCs.

Keywords:

Porous titanium dioxide, Dye sensitized solar cells, Refractive index calculation, Scattering, Optical characterization, FDTD simulation.

1. Introduction

Titanium dioxide is an n-type indirect band gap semiconductor. It has a wide range of applications due to its various optical, electrical and chemical characteristics [1-8]. Among the many TiO_2 modifications, the mesoporous structure is crucial in dye-sensitized solar cells (DSSCs) [9, 10] as well as perovskite solar cells (PSCs) [11, 12]. DSSCs contain two different semiconductor layers, the so-called mesoporous layer and the so-called blocking layer, as shown in Figure 1. While the first is essential for the charge separation, electron collection and ion conduction, the second is intended for suppressing the loss of generated electrons to the electrolyte. Both layers consist of the same chemical compound, TiO_2, but they have different mesostructures. For PSCs, the perovskite is deposited on a mesoporous particle TiO_2 structure for a better *I–V* characteristics [13].

The mesoporous particle TiO_2 films (mpp-TiO_2) of DSSCs are composed of nanoparticles in the range from 10 to 30 nm leading to a very large internal surface. Therefore, the amount of dye adsorbed in a DSSC is very high and an absorption capability of the dye to near 100% over a wide range of the visible spectral region is achieved. By virtue of comparison, the amount of adsorbed dyes on the surface of single crystals and poly-crystal materials is quite small, causing only about 1% absorption even at the peak wavelength [9]. On the other hand, the TiO_2 blocking layer of DSSCs, which we henceforth call the “compact layer” (compTiO_2), has only very small pores since it should block ion transport.

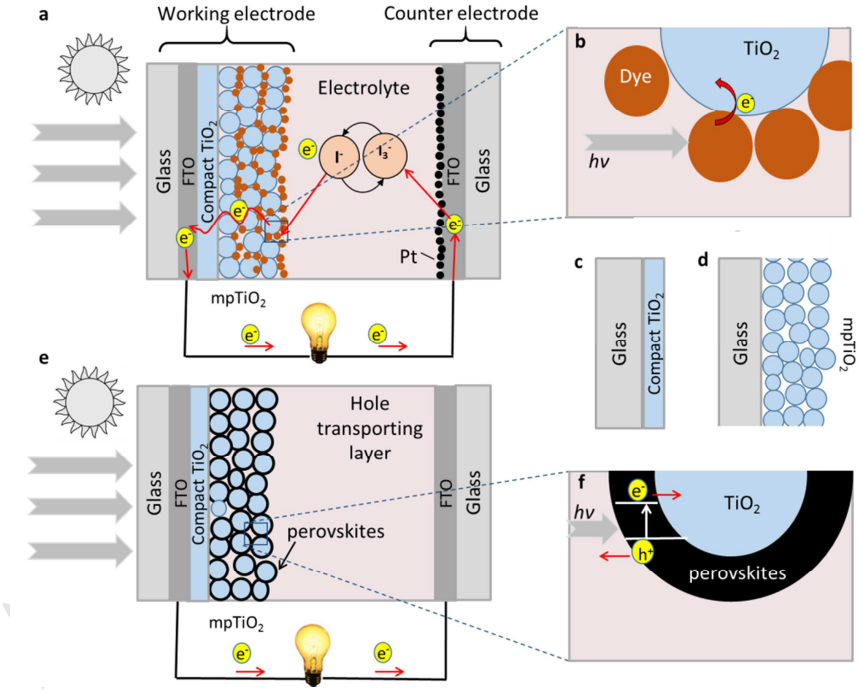

Figure 1: (a) Schematic of a DSSC with the operation principle and all optically relevant layers. (b) Photo-induced electron transfer in DSSC, (c) compact and (d) mesoporous particle TiO_2 layers on glass, investigated in this work. (e) Schematic of one kind of PSC with the operation principle and all optically relevant layers. (f) Photo-induced processes in this kind of PSC.

For PSCs, the use of a mesoporous particle TiO_2 layer was reported to improve the electron extraction, and promote the formation of a compact perovskite layer with large grains. Therefore, the performance of the PSCs is significantly improved [14]. Furthermore, the TiO_2-embedded perovskite films exhibit an improved long-term stability than the pristine perovskite films [14].

A crucial step in the numerical analysis of solar cells especially of DSSCs for optimization purposes is the use of appropriate optical models and material constants. Different deposition techniques and even various conditions for the same technique yield different microstructures and therefore different pore densities [15]. Since the refractive index of TiO_2 films is dependent on its density [16], several techniques were exploited to characterize TiO_2 layers [17-20]. Using capacitance-voltage measurements, the refractive permittivity of nanocrystalline TiO_2 thin films deposited on silicon using sol-gel spin coating was found to have a value of 25 [17]. Optical waveguide spectroscopy was used in [18] to follow the real-time diffusion of the dye N-719 dye into the mesoporous nanocrystalline TiO_2 films similar to those used in DSSCs. The experimental data were fitted to a value of 1.7942 for the refractive index of the porous TiO_2 before dye attachment. The inclusion of organic compounds in the fabrication process of TiO_2 films yielded an organic-TiO_2 nanocomposite that has a tunable refractive index between 1.76 and 2.05 at a wavelength of 589 nm [19]. All these works on TiO_2 films make clear that the determination of relevant optical parameters for solar cells (DSSCs and PCSs) has to be done exactly on these TiO_2 films fabricated with the solar cells-specific methods leading to specific porosities.

In this work, we introduce a detailed optical investigation for both the compTiO_2 and the mpp-TiO_2 films acting as blocking and active layers in DSSCs. Having accurate values for the porosity, the refractive index, the scattering and the thickness of the different TiO_2 layers is crucial for developing trustworthy simulation tools for DSSCs. Usually, estimated values of these parameters are used. Herein, efficient techniques are introduced to obtain the values of these parameters. In addition, the description of the optical scattering phenomena in these functionally important layers is improved.

2. Experimental details

In DSSCs, the thickness of the compTiO_2 layer is usually below 200 nm whereas that of the mpp-TiO_2 is in the range from 5 to 15 μm. Different fabrication techniques are used for each layer. The thin compTiO_2 samples used in this work were prepared with a sol-gel method via the spin-coating technique. This process is known to yield thin, homogeneous layers of controllable film morphology on numerous substrates [21]. It is widely used for DSSCs [22] as one possibility; alternatives are dip-coating (e.g. in [23]) or spray pyrolysis [24]. The thicker mpp-TiO_2 layers were fabricated using screen printing as in [25]. The alternative method of doctor blading (without a screen but with appropriate spacers) is expected to result in very similar films (e.g. in ref. [23]). A *JV* characteristics of a DSSC fabricated with the procedures below is given in the Supplementary Data section.

2.1 Fabrication of compact TiO_2 samples

In order to prepare a compTiO_2 film on a BK7 glass substrate [26], volumes of 250 µL of a precursor solution were dropped onto 2.5×2.5 cm^2 substrates placed in a spin coater (Spin150, SPS-Europe). The precursor solution was prepared at room temperature by mixing the titanium isopropoxide with ethanol and acetic acid as in [17]. A low spin-coating speed of 500 rpm at the beginning for 10 s enabled a uniform distribution of the solution across the sample, followed by a 3000 rpm step for 60 s with constant acceleration of 1000 rpm/s. Finally, the samples were heated in an oven within 60 min to 120 °C and remained for another 60 min at this temperature. Samples prepared as such have shown acceptable homogeneity in its interference color and the visually the same interference color when comparing different samples. The first sample (010-01) of the series (random selection) was taken for the further analysis. Sometimes, the influence of support surface roughness on the film properties is discussed. We have no indication for such an influence for our special deposition method. Therefore, we consider the properties of comp-TiO_2 on BK7 (as representative for many supports. BK7 has a roughness in the atomic range [26]) excluding any scattering effects from the BK7 surface.

To tune the thickness of the films, the deposition conditions were changed slightly, seeking for thicker layers leading to more pronounced Fabry-Perot oscillations. As examples three different samples were fabricated with lower rotation speed. The first sample (012-01) was coated for 6 s under a speed of 500 rpm and acceleration of 2000 rpm/s followed by 10 s under the speed of 2000 rpm with the same acceleration. The second sample (013-01) was coated for 6 seconds under a speed of 500 rpm and acceleration of 2000 rpm/s followed by 10 s under speed of 1000 rpm with 500 rpm/s acceleration. Finally, the third sample (014-01) was coated in the same way as the second one, but with a circular sample holder instead of the rectangular one used for the first two samples. In addition, multilayer deposition was used for sample 011-03 where 5 layers were deposited using the same procedure as for sample 014-01.

2.2 Fabrication of mmp-TiO_2 samples

In order to deposit mpp-TiO_2 films with a thickness between 5 to 15 µm the manual screen-printing method was used. The paste was the same as in ref. [23] and consisted of titania nanopowder, terpineol, ethyl cellulose, acetic acid, and isopropanol, mixed with the same procedure as in ref. [23] Here, five mpp-TiO_2 samples were prepared on glass substrates (BK7) and on quartz glass under the same conditions. The complex composition of the paste results from an optimizing process for the adjustment of titania surface termination, solid content, viscosity, and drying behavior.

2.3 Characterization

The optical characterization of the fabricated samples was done using a Cary 5G UV-Vis-NIR spectrometer against air as reference. The spectrometer was supplemented by a rotating stage as described in [27].

3. Results and discussion

3.1 Spectroscopic results for the different TiO_2 films

For the compact TiO_2 films, it can be observed (Figure 2a) that Fabry-Perot oscillations start to appear for the thickest samples making it possible to estimate the film thicknesses. An accurate determination of the film thickness must, however, be connected with a simultaneous determination of the refractive index. This will be calculated in the next section.

Regarding the mpp-TiO_2, the five samples were characterized using the UV-Vis-NIR spectrometer. Although the samples were fabricated according to the same procedure, significant fluctuations in their spectra can be observed in Figure 2b. We attribute these differences to thickness variations, as the manual screen printing method typically yields a layer thickness in a larger range [28].

The extinction spectrum ($E = -log_{10} T$ with T for the transmission) of one of these samples is shown in Figure 3. The starting wavelength is chosen to be 400 nm, so that the extinction curve reflects mainly the scattering due to this type of mesoporous layer with no absorption effects [29]. It's worth noting that the extinction that is directly determined from transmission data generally results from a superposition of absorption, reflection, and scattering effects.

3.2 The effective refractive index of the compact TiO_2 layer

In order to determine the effective refractive index of the compTiO_2 layer, a published technique [27] based on spectral transmission (T-λ) measurements with different angle of incidence was adopted. The transmission spectra for seven different angles of incidence for perpendicularly polarized light (s-pol.) as function of wave number k, are shown in Figure 4. These curves show distinct Fabry-Perot resonances due to reflections at the thin film boundaries. It is observed, that these oscillating curves start to be distorted as the angle of incidence increases, leading to two extrema (i.e. one maximum and one minimum) in the case of 60° instead of three at other angles of incidence. A jump at 800 nm ($k = 12.5 \cdot 10^3$ cm^{-1}) emerges at increasing angles of incidence, which is due to the detector change in the spectrometer that is not fully compensated because of the beam displacement in our modified setup. Another jump observed in the spectra at 360 nm originates from the source change from the visible to the ultraviolet lamp. The influence of this jump is excluded in Fig. 4 by restricting the regarded spectral range to larger wavelengths (larger than 360 nm, $k < 27.7 \cdot 10^3$ cm^{-1}), as the range of smaller wavelengths has absorptions and is not well suited for Fabry-Perot analysis.

As known (see e.g. [27, 30]), the positions of the interference extrema (i.e. of the maxima and minima) on the wavenumber scale (k_{ext}) show a linear dependence on the extremum number (M_a). This number is correlated with the usual [30] interference order N by a linear relationship: $2N = M_a + M_o$, where the offset (M_o) depends on the specific measurement technique. Whereas the interference order is usually the difference between the number of wavelengths in two consecutive light paths, the extremum numbers ($M_a + M_o$) are the difference between the numbers of half wavelengths in these paths.

Accordingly, the k_{ext}-M_a dependence was fitted with a straight line for each angle of incidence as shown in Figure 5. Also the maximal and minimal possible values were estimated for the error

determination. The slope m of this line delivers the thickness-dependent part of the optical path difference $\Delta_d = (2m)^{-1}$. It differs from the total path difference Δ by the phase jump due to the reflection on the optically dense-to-thin interface: $\Delta = \Delta_d + \lambda/2$. The dependence of Δ_d on the incidence angle α for s-polarized light is given by $\Delta_d = 2d\sqrt{n^2 - sin^2\alpha}$ and is plotted in Figure 6. Here, a linear relationship must be valid based on the laws of classical wave optics. Therefore, the experimental points were fitted with a linear curve and all deviations are ascribed to measurement errors. This induces the error in the refractive index and in the thickness. As a result, the refractive index for the compTiO$_2$ was determined to be 1.7982 ± 0.005, while the thickness was found to be (264.0 ± 1.5) nm.

The refractive index determined from this sample can now be used as an input parameter for a fast and accurate thickness determination of all samples made by the described fabrication technique. Such investigations reveal the expected dependence of the thickness on the spin-coating rotation speed, but also a surprisingly high influence of other fabrication parameters (e.g. the support shape) on the thickness. Since these influences affect a geometrical parameter only and leave the fabricated material unchanged, we shift this topic to future works. The wavelength dependence of the refractive index will be discussed in Section 3.4.

a

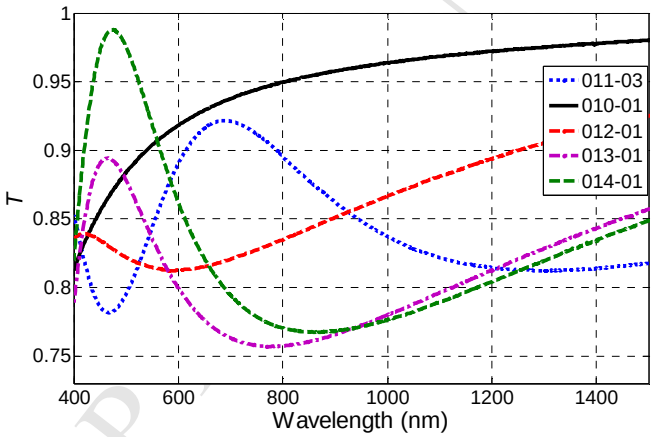

b

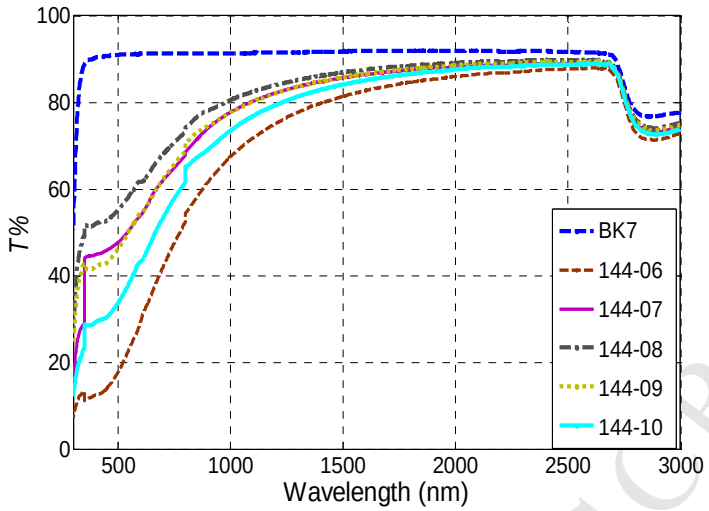

Figure 2: (a) Transmission spectra for the compTiO_2 layer for different spin coating procedures. The oscillations result from an interplay between Fabry-Perot resonances and absorption effects. (b) Transmission spectra for mpp-TiO_2 layers on glass substrates for the different samples of one batch. The discontinuities at 360 nm and 800 nm are due to lamp and detector changes, respectively.

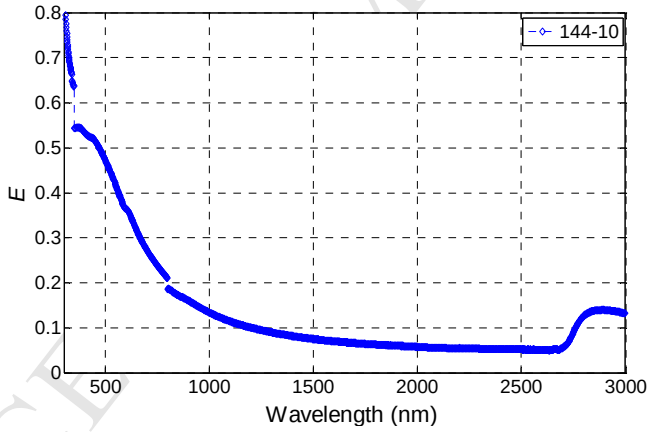

Figure 3: Extinction spectrum of the mpp-TiO_2 layer, sample 144-10. The discontinuities at 360 nm and 800 nm are due to lamp and detector changes, respectively.

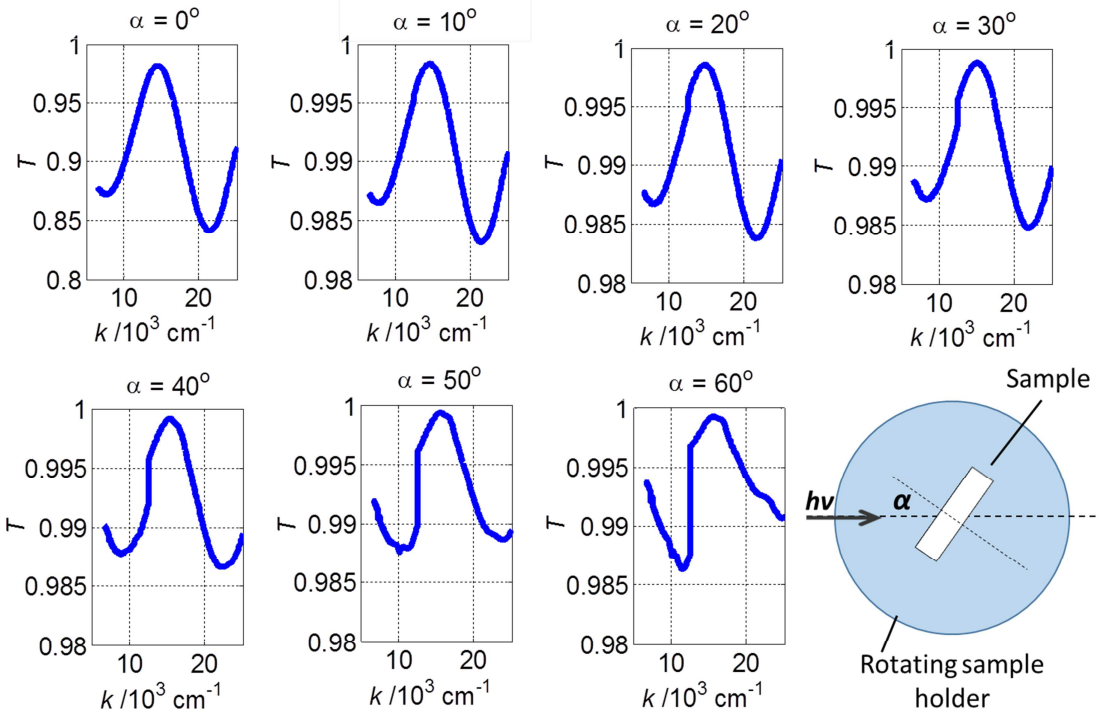

Figure 4: The optical transmission spectrum of a compTiO$_2$ layer at different angles of incidence for sample 011-03. The drawing (bottom, right) shows the experimental setup.

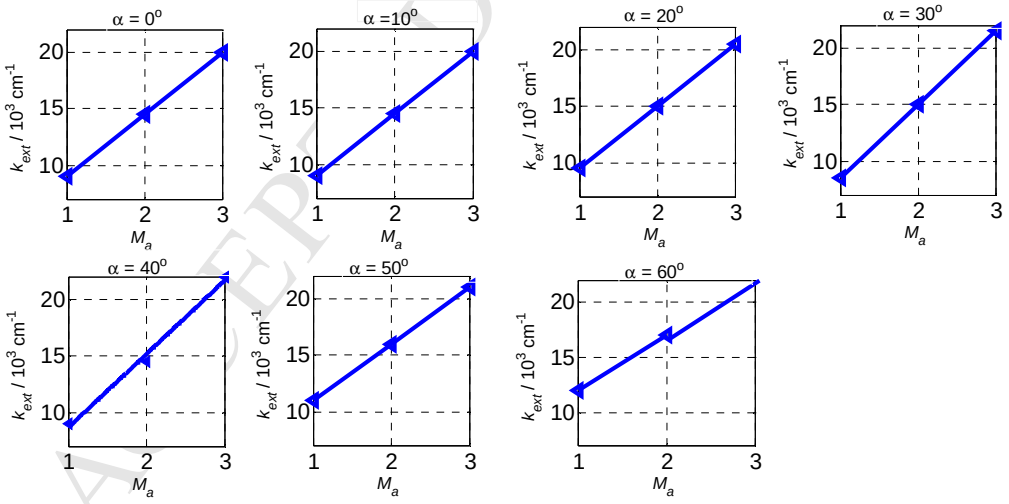

Figure 5: The extremum positions (i.e. maximum and minimum position) in the transmission spectrum versus extremum number (see text) for all observed extrema at different angle of incidence.

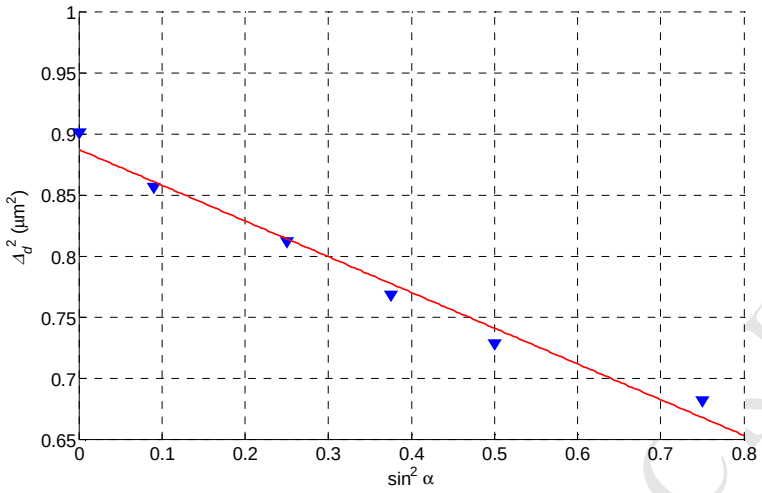

Figure 6: The square of the optical path difference Δ_d versus $\sin^2\alpha$. The line represents a linear fit.

3.3. The effective refractive index of the mesoporous particle layer

The transmission spectrum of the mpp-TiO_2 films (Figure 2b) shows a completely different behavior compared to the compact films (Figure 2a). No Fabry-Perot oscillations are visible; instead there is a big part of the extinction which is obviously caused by scattering. Therefore, the angular-dependent spectral transmission (T-λ) method for determining the effective refractive index used above cannot be applied for the mesoporous layer. However, one can recognize a part in the spectrum (between 2000 and 2700 nm) where the extinction is low and nearly constant. We ascribe this low extinction to the reflection loss at the sample support (Figure 7). However, the support is in physical contact with the mpp-TiO_2 and, therefore, this reflection loss is influenced by the properties of the mpp-TiO_2. We have used the Fresnel formula for describing this effect from which we calculated the effective refractive index.

The transmitted power, T_{SRL}, where SRL stands for support reflection loss, is thus calculated using:

$$T_{SRL} = 1 - R_{BK7} - R_{mp/BK7} \quad (1)$$

$$R_{BK7} = \left(\frac{n_{BK7}-1}{n_{BK7}+1}\right)^2 \quad (2)$$

$$R_{mp/BK7} = \left(\frac{n_{mp}-n_{BK7}}{n_{mp}+n_{BK7}}\right)^2 \quad (3)$$

where R_{BK7} is the reflectance between air and the glass substrate (BK7), $R_{mp/BK7}$ stands for the reflectance between the BK7 and the mesoporous layer, and n_{mp} is the effective refractive index of mpp-TiO_2. The value of R_{BK7} is equal to 0.04 [26]. This value was verified in the

measurements shown in Figure 2b where the transmission of a normal BK7 glass layers from front and back side was found equal to 0.92. Solving the second order equation in n_{mp} resulting from (1)-(3), two values for the refractive indexes were found: 1.463 and 1.625.

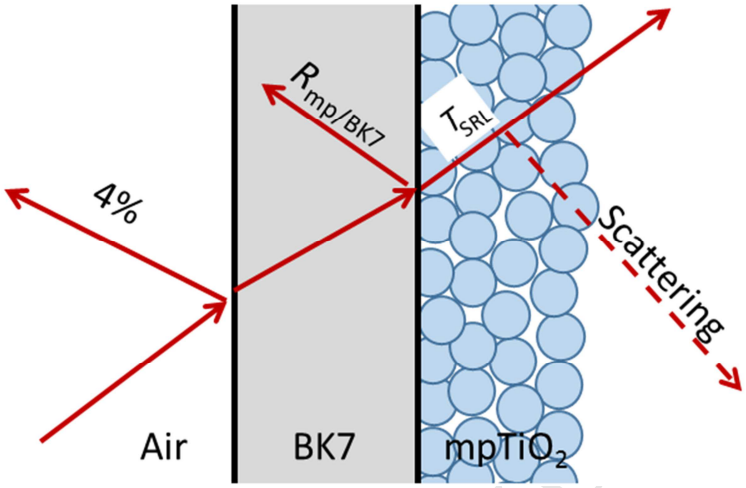

Figure 7: Schematic of the supported mesoporous Titania films used for calculating the support reflection loss (SRL)

To pick up the correct value from the two determined results, and for verifying the measurements, the same experiment was repeated on a quartz substrate instead of BK7. The same set of equations ((1)-(3)) was used (but with replacing BK7 by quartz glass). The refractive index of quartz glass is 1.46 [26]. Solving the equation to get n_{mp} , these two values were found: 1.621 and 1.315. Since only one of these values is delivered from both experiments with small deviation from each other (1.623 ± 0.002), we rule out the other results. Repeating the same procedure on five samples (144-06 to 144-10), the mesoporous particle layer refractive index was found to be in the range of 1.628 ± 0.006. Obviously, the unavoidable fluctuations in the manual screen printing technique used here did not affect the effective refractive index much. The obtained value refers to the used particle size and fabrication technique. By changing the particles size or deposition technique, new values should be expected [31]. However, other parameters such as support surface treatment will only have a soft influence on the optical properties of the film. Such influences are a principle difficulty for all tunable materials.

In order to calculate the porosity (*P*) of the film, a linear dependence between the porosity (*P*) and the square of the refractive index (i.e. the relative permittivity ε), was assumed. Giving that $\varepsilon = \varepsilon' + j\varepsilon''$, where ε' and ε'' are the real and imaginary part of the permittivity respectively, the following mixing rule with respect to the porosity and the real part of the background refractive index is assumed:

$$\varepsilon' = \varepsilon'_B - P\left(\varepsilon'_B - 1\right) \tag{4}$$

where ε'_B is the real part of the permittivity of the background bulk TiO_2 ($\varepsilon'_B = 5.75$) (at λ =550 nm) [32]. Applying equation (4), the porosity of the mesoporous layer is found to be (65.2 ± 0.2) %. A comparison of this value with adsorption data is challenging because of the film geometry

of the sample and the weight of the support. Possibly, reliable data can be obtained by Kr adsorption measurements [33].

3.4. Dispersion and absorption of the compact TiO_2

Up to now, dispersion and absorption of the films were neglected. However, the data for the compact layer enable a well-based prediction of these effects. For that, we determine the porosity of the films. The value 53.5% is found using the same approximation as in the last section with the refractive index determined as in section 3.2. We use this porosity value and literature data of the bulk material [34]. for calculating the parameters of the porous system applying the simple mixing rule given in equation (4). A Lorentz-Drude (LD) fitting model as developed in [35] was applied to the background material (TiO_2), allowing easy data handling in future DSSC simulations. Figure 8a shows the achieved result

For describing the absorption of the compTiO_2 layer, the imaginary part of the refractive index is estimated based on the absorption data in [34] and by applying the same effective medium approximation as in (4). This approximation implies the same mixing rule between the porosity and the imaginary part of the permittivity given by: $\varepsilon'' = \varepsilon_B'' - P\varepsilon_B''$, where ε_B'' represents the imaginary part of the permittivity for the bulk TiO_2 and P is the porosity as calculated above. Again, LD fitting is used and the results for ε'' are shown in Figure 8b.

3.5. Scattering in the compact layer

To simulate light interaction within a compact layer on a glass substrate, we used the finite difference time-domain (FDTD) algorithm. For the implementation of the numerical layer model, we adopted the open-source FDTD platform embedded in MEEP [36]. The simulated volume is chosen to be 100 μm × 100 μm × 100 μm with a calculating grid of 10 nm × 10 nm × 10 nm and the resolution is set to 10, (i.e. 10 meshes per calculating grid).

Figure 9 shows the simulation result in comparison with the measurement. One can see a small mismatch between the measured transmission spectrum of sample 011-03 and its simulation using the optical parameters calculated in the previous sections. The simulated layer thickness is chosen to be 264 nm. The apparent mismatch seems to be constant between the wavelengths 500 nm and 2000 nm. As this region is free of any absorption in TiO_2 as shown in Figure 8b and reported in the literature [29], we consider this mismatch to be due to scattering.

In general, scattering may be associated to surface or volume scattering. Surface scattering is most probably due to the roughness of the surface while bulk scattering is usually related to interaction with disturbances inside the layer. According to the surface roughness measured in [27, 37], the samples show a very flat surface over the whole film, with a root mean square (RMS) roughness around 0.50 nm in a $(0.5\ \mu m)^2$ region. Therefore, a bulk scattering model is more likely for the compact layer.

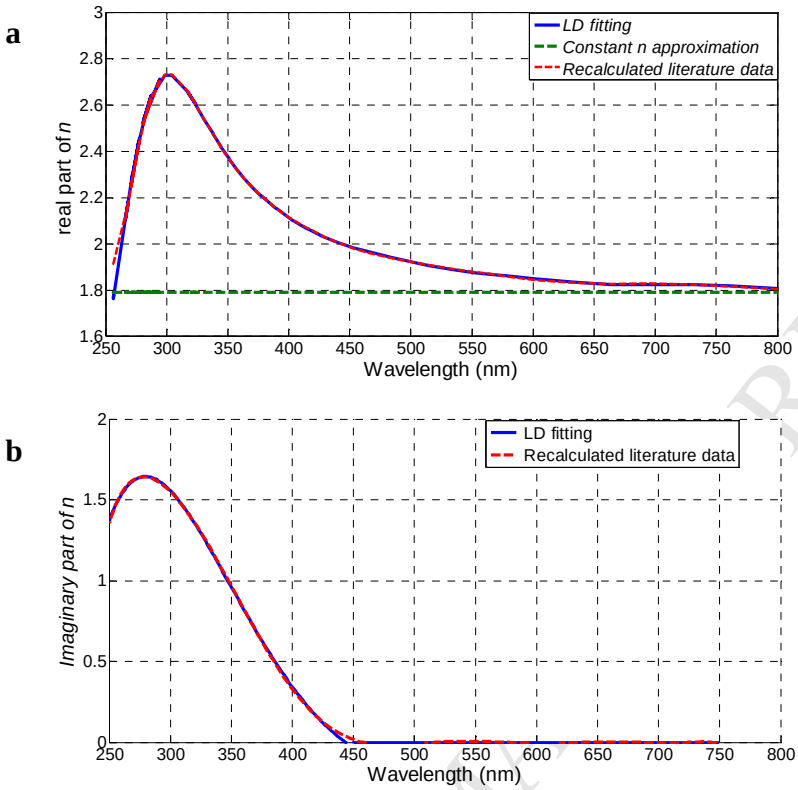

Figure 8: (a) Dispersion of compTiO$_2$ based on ref. [28]. (b) Imaginary part of the refractive index versus wavelength for a compTiO$_2$ layer based on ref. [28]. The LD fitting parameters for (a) and (b) are: ε_∞= 1, σ_1 = 2.4221e+41, ω_1= 0.13145, Γ_1= 0.011715, σ_2= 8.9217. ω_2= 0.64888, Γ_2= 5.2313, σ_3= 0.50133, ω_3= 3.6165, and Γ_3= 0.85456, according to the model in [35].

Many models for bulk scattering have been described in the literature [38, 39]. Rayleigh and Mie scattering are two of the simplest models for volume scattering effects ascribed to single particles of special properties. Wavelength-independent scattering is another simplified description useful for scattering events from objects much larger than the wavelength. Mathematically their introduction can be easily done by adding a wavelength-independent part to the imaginary part of the refractive index [40].

To explore the influence of this simple volume scattering model, an additional simulation parameter is introduced in the imaginary part of the refractive index, so that the complex refractive index of the compact layer becomes $n + j\,(K + K_{sca})$, where K_{sca} is the new parameter. We introduce the scattering parameter in the n-model instead of an ε-model because this is more near to the physical process of scattering losses resulting in an exponential decay of intensity. A little surprisingly, this single additional parameter leads to a perfect fitting between simulation and experimental data in the whole spectrum as shown in Figure 9 (dotted line) for a value of K_{sca} = 0.20384.

3.6. Scattering in the mesoporous layer

Let us choose the region of interest for the optical investigation of the mpTiO_2 layer to extend to the wavelength range from 450 nm to 2500 nm where no absorption is observed. Therefore, we can ascribe the reflection-corrected extinction spectrum shown in Figure 10 (dotted line) to scattering effects only.

For the mpp-TiO_2, the scattering is clearly wavelength-dependent. Therefore, the applied model for the compact layer is not valid here. The extinction spectrum is used in describing the scattering within the mpp-TiO_2 layer instead of the transmission spectrum used for the CompTiO_2 layer because the logarithmic scale is better suited for displaying the large intensity changes and because known microscopic scattering models deliver this value. The accurate description of the scattering of a mesoporous film is, however, difficult and requires detailed information of the underlying micro structure. Therefore, we use the Mie model [38, 39] as simple phenomenological description of the wavelength-dependent scattering effects. The parameters of the model have to be regarded as effective parameters with restricted physical meaning. A Matlab-based Mie scattering model in [41] was therefore applied on the extinction data where two fitting parameters have to be adjusted, namely the effective scattering particle radiusand the scattering prefactor. The scattering prefactor is an aggregated parameter that depends on the effective scattering particle density, the scattering layer thickness, and the aperture of the spectrometer detector.

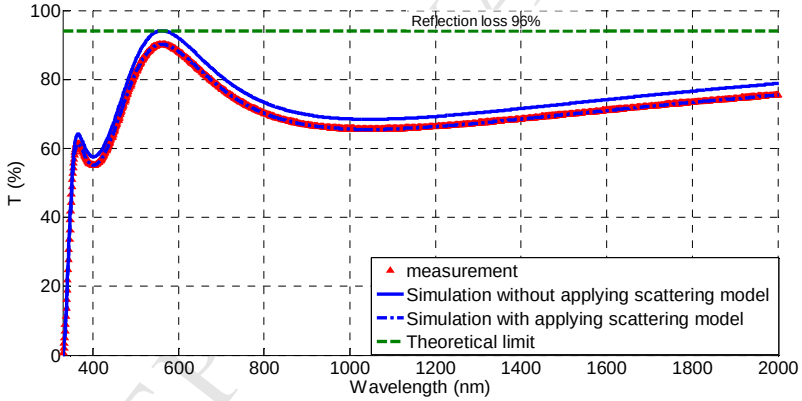

Figure 9: Measurements versus simulation transmission spectrum for a compact layer (sample 011-03)

In order to capture the required fitting parameter for the Mie scattering model, a fitting procedure was applied using Matlab [41]. The fitting process was affected by the jump in the measured extinction curve at 800 nm. This jump is due to the change of the detector made by the UV-Vis spectrometer, where a UV-Visible detector is replaced by an infrared one. To overcome the discontinuity and to obtain more accurate fitting results, we divided our extinction curve into two regions of interest. The first is from 450 nm to 800 nm, while the second is from 800 nm to 2500 nm. Each of these regions is then fitted independently.

The fitting was made on a sample on BK7. The effective scattering particle radius in both regions was found to be 46.5 nm with an error of about 2.5 nm in the two regions, respectively. The constant radius in the two regions is compensated by the variation in the prefactor

parameter. The surprisingly high agreement between the measured and the simulated data is shown in Figure 10. To verify the results, we repeated the analysis for mpTiO_2 on a quartz glass support. The same effective scattering particle radius was found but with other values for the scattering prefactor.

This invariant radius of effective scattering particle is expected as in both samples, the scattering occurs due to the same scattering medium. The different prefactors reflect the use of two different spectrometer detectors with two different aperture values and differences in the sample thickness from one sample to another, due to the use of a manual deposition technique. Therefore, we consider the 46.5 nm as a well-justified value for the radius of the effective scattering particles in the mpp-TiO_2 layer. This value can be used in future simulation of the scattering effects in conjunction with the Mie scattering model. However, it should be noted that it is not directly correlated to the actual particle radius in the mpp-TiO_2 film.

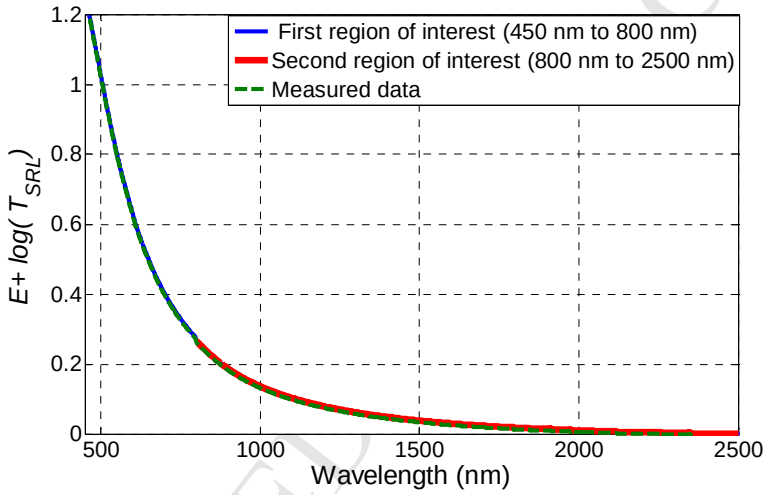

Figure 10: Fitting model based on Mie scattering for mpTiO_2 on a BK7 support. T_{SRL} represents the transmission due to the SRL.

4. Conclusions

The optical properties of compTiO_2 and mpp-TiO_2 films differ strongly from those of ordinary TiO_2. The porosity of the solid and the scattering by inhomogeneities determine their characteristic behavior.

Using spectrally resolved transmission measurements, the refractive index of the compTiO_2 film was determined to be 1.7982 ± 0.005. For the mpp-TiO_2 layer where scattering effects are dominate, the effective refractive index was determined using the reflection loss, yielding a value of 1.62 ± 0.002. Assuming a simple mixing rule for the effective permittivity of the pours TiO_2, the porosity of the compact layer was determined to be 53.5%, while that of the mesoporous layer is 65.2%.

In order to account for the mismatch due to scattering between the measured transmission spectrum of compTiO_2 and its simulation, a damping constant was introduced in the imaginary part of the refractive index to account for the frequency-independent scattering and found to describe the experimental data well. In the case of the mpp-TiO_2 layer, a Mie scattering model was found to be best suited to describe the frequency-dependent extinction spectrum. The radius of the effective scattering particles of 46.5 nm describes the data well and is in the same order of magnitude as the pore size of the layer. Therefore, we can conclude that the optical transport in these layers is determined by the intentional nanostructure and not by µm-scale defects occasionally occurring in these films.

The remarkably high porosity of the two investigated layers can also be expected to have a large influence on the ionic transport, on the charge screening, and on the mutual interaction of different kinds of charges in these semiconductors. For an understanding of that, data on pore sizes and interconnectivities are needed.

5. Acknowledgments

The experimental part of this work was carried out at the MPI für Kohlenforschung. It was supported by Dr. M. Muldarisnur and D. Naumann. This work was financially supported by the German Academic Exchange Service (DAAD) in the project SURYS as well as by the cluster of excellence RESOLV. The authors acknowledge the valuable support of Prof. M. Ulbricht, Dr. M. Eisinger and S. Kustos. We would also like to acknowledge the support of The World Academy of Sciences (TWAS) for providing the necessary computational resources.

Appendix A. Supplementary data

Supplementary data related to this article can be found at XXXX

References

[1] V. Anitha, A.N. Banerjee, S.W. Joo, Recent developments in TiO2 as n-and p-type transparent semiconductors: synthesis, modification, properties, and energy-related applications, J Mater Sci, 50 (2015) 7495-7536.
[2] A. Gupta, S. Varshney, A. Goyal, P. Sambyal, B. Kumar Gupta, S.K. Dhawan, Enhanced electromagnetic shielding behaviour of multilayer graphene anchored luminescent TiO2 in PPY matrix, Materials Letters, 158 (2015) 167-169.
[3] Z. Pei, S. Weng, P. Liu, Enhanced photocatalytic activity by bulk trapping and spatial separation of charge carriers: A case study of defect and facet mediated TiO2, Applied Catalysis B: Environmental, 180 (2016) 463-470.
[4] M. Kettunen, R.J. Silvennoinen, N. Houbenov, A. Nykänen, J. Ruokolainen, J. Sainio, V. Pore, M. Kemell, M. Ankerfors, T. Lindström, M. Ritala, R.H.A. Ras, O. Ikkala, Photoswitchable Superabsorbency Based on Nanocellulose Aerogels, Advanced Functional Materials, 21 (2011) 510-517.
[5] B. Cho, T.-W. Kim, M. Choe, G. Wang, S. Song, T. Lee, Unipolar nonvolatile memory devices with composites of poly(9-vinylcarbazole) and titanium dioxide nanoparticles, Organic Electronics, 10 (2009) 473-477.

[6] B.O. Aduda, P. Ravirajan, K.L. Choy, J. Nelson, Effect of morphology on electron drift mobility in porous TiO2, International Journal of Photoenergy, 6 (2004) 141-147.
[7] A. Soklič, M. Tasbihi, M. Kete, U.L. Štangar, Deposition and possible influence of a self-cleaning thin TiO2/SiO2 film on a photovoltaic module efficiency, Catalysis Today, 252 (2015) 54-60.
[8] X. Xue, J. Qin, J. Song, J. Qu, Y. Shi, W. Zhang, Z. Song, L. Jiang, J. Li, H. Guo, T. Zhang, The methods for creating energy efficient cool gray building coatings—Part I: Preparation from white and black pigments, Solar Energy Materials and Solar Cells, 130 (2014) 587-598.
[9] B. O'Regan, M. Gratzel, A low-cost, high-efficiency solar cell based on dye-sensitized colloidal TiO2 films, Nature, 353 (1991) 737-740.
[10] N.G. Park, G. Schlichthörl, J. van de Lagemaat, H.M. Cheong, A. Mascarenhas, A.J. Frank, Dye-Sensitized TiO2 Solar Cells: Structural and Photoelectrochemical Characterization of Nanocrystalline Electrodes Formed from the Hydrolysis of TiCl4, The Journal of Physical Chemistry B, 103 (1999) 3308-3314.
[11] M.A. Loi, J.C. Hummelen, Hybrid solar cells: perovskites under the sun, Nature materials, 12 (2013) 1087.
[12] A. Apostolopoulou, D. Sygkridou, A. Kalarakis, E. Stathatos, High Efficiency Perovskite Solar Cells Fabricated under Ambient Conditions with Mesoporous TiO2/In2O3 Scaffold, World Academy of Science, Engineering and Technology, International Journal of Electrical, Computer, Energetic, Electronic and Communication Engineering, 11 (2017) 113-116.
[13] F. Giordano, A. Abate, J.P.C. Baena, M. Saliba, T. Matsui, S.H. Im, S.M. Zakeeruddin, M.K. Nazeeruddin, A. Hagfeldt, M. Graetzel, Enhanced electronic properties in mesoporous TiO2 via lithium doping for high-efficiency perovskite solar cells, Nature communications, 7 (2016).
[14] D. Wei, J. Ji, D. Song, M. Li, P. Cui, Y. Li, J.M. Mbengue, W. Zhou, Z. Ning, N.-G. Park, A TiO 2 embedded structure for perovskite solar cells with anomalous grain growth and effective electron extraction, Journal of Materials Chemistry A, (2017).
[15] Amorphous TiO2 films with high refractive index deposited by pulsed bias arc ion plating, Surface and Coatings Technology, 201 (2007) 7252-7258.
[16] Density and refractive index of TiO2 films prepared by reactive evaporation, Thin Solid Films 371 (2000) 218-224.
[17] M. Kumar, M. Kumar, D. Kumar, The deposition of nanocrystalline TiO2 thin film on silicon using Sol–Gel technique and its characterization, Microelectronic Engineering, 87 (2010) 447-450.
[18] A. Peic, D. Staff, T. Risbridger, B. Menges, L.M. Peter, A.B. Walker, P.J. Cameron, Real-Time Optical Waveguide Measurements of Dye Adsorption into Nanocrystalline TiO2 Films with Relevance to Dye-Sensitized Solar Cells, The Journal of Physical Chemistry C, 115 (2011) 613-619.
[19] R. Himmelhuber, P. Gangopadhyay, R.A. Norwood, D.A. Loy, N. Peyghambarian, Titanium oxide sol-gel films with tunable refractive index, Optical Materials Express, 1 (2011) 252-258.
[20] S. Muhammad Rizwan, H. Seppo, T. Jari, Thermal properties of TiO 2 films fabricated by atomic layer deposition, IOP Conference Series: Materials Science and Engineering, 60 (2014) 012008.

[21] I. Sta, M. Jlassi, M. Hajji, M. Boujmil, R. Jerbi, M. Kandyla, M. Kompitsas, H. Ezzaouia, Structural and optical properties of TiO2 thin films prepared by spin coating, Journal of Sol-Gel Science and Technology, 72 (2014) 421-427.
[22] S.-M. Paek, H. Jung, Y.-J. Lee, N.-G. Park, S.-J. Hwang, J.-H. Choy, Nanostructured TiO 2 films for dye-sensitized solar cells, Journal of Physics and Chemistry of Solids, 67 (2006) 1308-1311.
[23] F. Marlow, A. Hullermann, L. Messmer, Is the Charge Transport in Dye□Sensitized Solar Cells Really Understood?, Advanced Materials, 27 (2015) 2447-2452.
[24] M. Okuya, K. Nakade, D. Osa, T. Nakano, G.A. Kumara, S. Kaneko, Fabrication of dye-sensitized solar cells by spray pyrolysis deposition (SPD) technique, Journal of Photochemistry and Photobiology A: Chemistry, 164 (2004) 167-172.
[25] S. Ito, P. Chen, P. Comte, M.K. Nazeeruddin, P. Liska, P. Pechy, M. Grätzel, Fabrication of screen□printing pastes from TiO2 powders for dye□sensitised solar cells, Progress in photovoltaics: research and applications, 15 (2007) 603-612.
[26] N.P. Bansal, R.H. Doremus, Handbook of glass properties, Elsevier2013.
[27] D. Konjhodzic, H. Bretinger, F. Marlow, Structure and properties of low-n mesoporous silica films for optical applications, Thin Solid Films, 495 (2006) 333-337.
[28] K. Fan, M. Liu, T. Peng, L. Ma, K. Dai, Effects of paste components on the properties of screen-printed porous TiO2 film for dye-sensitized solar cells, Renewable Energy, 35 (2010) 555-561.
[29] S.-Y. Du, Z.-Y. Li, Enhanced light absorption of TiO 2 in the near-ultraviolet band by Au nanoparticles, Opt. Lett., 35 (2010) 3402-3404.
[30] E. Hecht, Optics, Addison Weley, (2002).
[31] S.Y. Chae, M.K. Park, S.K. Lee, T.Y. Kim, S.K. Kim, W.I. Lee, Preparation of size-controlled TiO2 nanoparticles and derivation of optically transparent photocatalytic films, Chemistry of Materials, 15 (2003) 3326-3331.
[32] A. Wypych, I. Bobowska, M. Tracz, A. Opasinska, S. Kadlubowski, A. Krzywania-Kaliszewska, J. Grobelny, P. Wojciechowski, Dielectric Properties and Characterisation of Titanium Dioxide Obtained by Different Chemistry Methods, Journal of Nanomaterials, 2014 (2014) 9.
[33] K. Wessels, M. Minnermann, J. Rathousky, M. Wark, T. Oekermann, Influence of Calcination Temperature on the Photoelectrochemical and Photocatalytic Properties of Porous TiO2 Films Electrodeposited from Ti(IV)-Alkoxide Solution, The Journal of Physical Chemistry C, 112 (2008) 15122-15128.
[34] M. Smietana, M. Koba, E. Brzozowska, K. Krogulski, J. Nakonieczny, L. Wachnicki, P. Mikulic, M. Godlewski, W.J. Bock, Label-free sensitivity of long-period gratings enhanced by atomic layer deposited TiO 2 nano-overlays, Optics express, 23 (2015) 8441-8453.
[35] S. Abdellatif, R. Ghannam, A. Khalil, Simulating the dispersive behavior of semiconductors using the Lorentzian–Drude model for photovoltaic devices, Applied optics, 53 (2014) 3294-3300.
[36] A.F. Oskooi, D. Roundy, M. Ibanescu, P. Bermel, J. Joannopoulos, S.G. Johnson, MEEP: A flexible free-software package for electromagnetic simulations by the FDTD method, Computer Physics Communications, 181 (2010) 687-702.
[37] D. Konjhodzic, H. Bretinger, U. Wilczok, A. Dreier, A. Ladenburger, M. Schmidt, M. Eich, F. Marlow, Low-n mesoporous silica films: structure and properties, Appl. Phys. A, 81 (2005) 425-432.

[38] M. Born, E. Wolf, Principles of optics: electromagnetic theory of propagation, interference and diffraction of light, CUP Archive2000.
[39] M. Kerker, The scattering of light and other electromagnetic radiation: physical chemistry: a series of monographs, Academic press2013.
[40] R. Levinson, P. Berdahl, H. Akbari, Solar spectral optical properties of pigments—Part I: model for deriving scattering and absorption coefficients from transmittance and reflectance measurements, Solar energy materials and solar cells, 89 (2005) 319-349.
[41] C. Mätzler, MATLAB functions for Mie scattering and absorption, version 2, IAP Res. Rep, 8 (2002).

Refractive Index and Scattering of Porous TiO_2 Films

Highlights

- Reliable methods for the determination of the refractive index of different TiO_2 films used in solar cells are described.
- Refractive index values for two titania films typically used in solar cells: 1.7982 and 1.62
- Porosities of these two titania typically used in solar cells: 53.5 % and 65.2 %
- Effective scattering particle radius in one solar-cell related titania film: 46.5 nm